Acta Cryst A FOUNDATIONS ADVANCES
ISSN 2053-2733

Temperature- and energy-dependent phase shifts of resonant multiple-beam X-ray diffraction in germanium crystals

Po-Yu Liao,[a] Wen-Chung Liu,[a] Chih-Hao Cheng,[a] Yi-Hua Chiu,[a] Ying-Yu Kung[a] and Shih-Lin Chang[a,b]*

[a]Department of Physics, National Tsing Hua University, Hsinchu, Taiwan, and [b]National Synchrotron Radiation Research Center, Hsinchu, Taiwan. *Correspondence e-mail: slchang@nsrrc.org.tw

Received 25 February 2015
Accepted 10 May 2015

Edited by H. Schenk, University of Amsterdam, The Netherlands

Keywords: resonant phase shifts; temperature dependence; energy dependence; X-ray multiple diffraction; Ge crystals.

This paper reports temperature- and energy-dependent phase shifts of resonant multiple-beam X-ray diffraction in germanium crystals, involving forbidden (002) and weak (222) reflections. Phase determination based on multiple-beam diffraction is employed to estimate phase shifts from (002)-based {(002)(375)(37$\bar{3}$)} four-beam cases and (222)-based {(222)($\bar{5}$3$\bar{3}$)} three-beam cases in the vicinity of the Ge *K* edge for temperatures from 20 K up to 300 K. The forbidden/weak reflections enhance the sensitivity of measuring phases at resonance. At room temperature, the resonance triplet phases reach a maximum of 8° for the four-beam cases and −19° for the three-beam cases. It is found that the peak intensities and triplet phases obtained from the (002) four-beam diffraction are related to thermal motion induced anisotropy and anomalous dispersion, while the (222) three-beam diffraction depends on the aspherical covalent electron distribution and anomalous dispersion. However, the electron–phonon interaction usually affects the forbidden reflections with increasing temperatures and seems to have less effect on the resonance triplet phase shifts measured from the (002) four-beam diffraction. The resonance triplet phase shifts of the (222) three-beam diffraction *versus* temperature are also small.

1. Introduction

X-ray diffraction at resonant photon energies, namely atomic absorption edges, sometimes called X-ray resonant diffraction, is frequently used to study the structural and magnetic properties of solids. Resonance occurs when the incident photon energy approaches the value of an absorption edge of a constituent atom and excites an inner-shell electron to an unoccupied state of the outer shell. The outer shell of the atom is strongly coupled with its neighbouring atoms and thereby the atomic scattering factor becomes anisotropic. This kind of reflection is also called an ATS reflection (anisotropy of the tensor of susceptibility) (Templeton & Templeton, 1980; Dmitrienko, 1983, 1984; Kokubun *et al.*, 2004; Colella & Shen, 2006) and violates the extinction rules for glide planes and/or screw axes. Space-group symmetry forbidden reflections then become measurable. On the other hand, the electronic states of atoms in solids are also bound up with thermal atomic motion. The so-called thermal motion induced anisotropy of the X-ray susceptibility also appears in crystals (Dmitrienko, 1983; Dmitrienko *et al.*, 1999; Dmitrienko & Ovchinnikova, 2000). The electron density of the resonant atom is distorted by the surrounding atoms and the atomic positions deviate from their equilibrium positions. Usually, the atomic motion in solids is much slower than that of the electrons. This implies

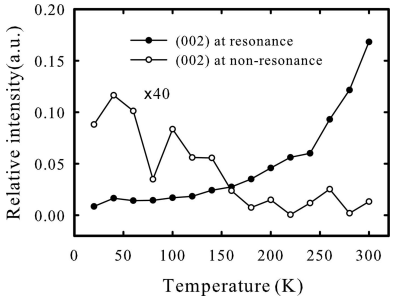

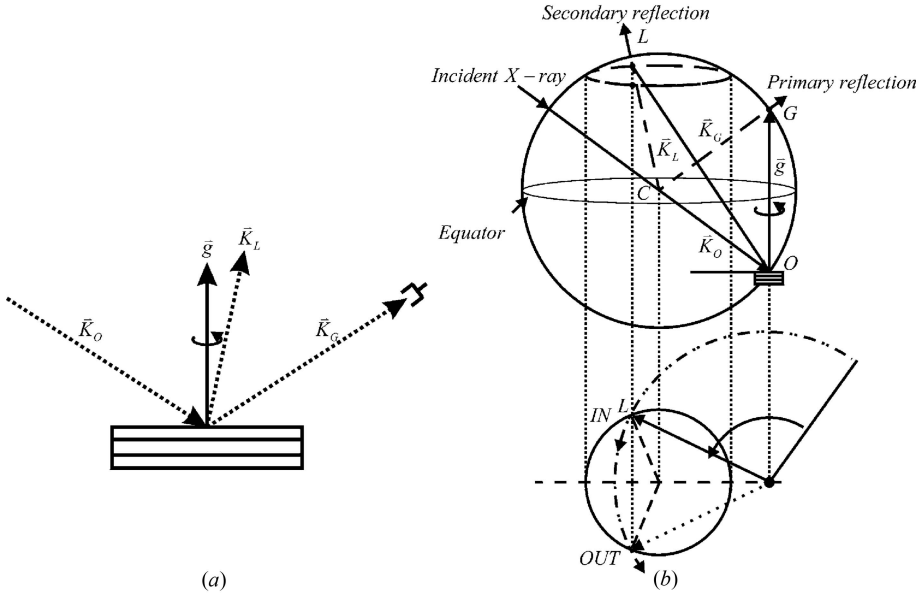

Figure 1
The geometry of a Renninger scan in the (*a*) real space and (*b*) reciprocal space.

that the intensity of the forbidden reflection at resonance is related to the electron–phonon interaction. When the temperature rises, the electron density of the resonant atom is distorted considerably and the temperature factor boosts the intensity of the forbidden reflection in the vicinity of the resonant energy. Based on the symmetry considerations (Kokubun *et al.*, 2001; Kirfel *et al.*, 2002), a situation occurs in which a resonant atom is located at a position possessing a high symmetry and the anisotropic structure vanishes in the dipole–dipole interaction. Under such circumstances, the forbidden reflection can be excited in a high-order situation, the so-called dipole–quadrupole interaction (Templeton & Templeton, 1994; Dmitrienko *et al.*, 1999). The resonant atom moves among the neighbouring atoms or the positions of the neighbouring atoms are changed due to their relative motions. The symmetry is then lowered at the instantaneous motion of atoms and the electronic state in the atoms becomes distorted. Therefore, the configuration of the reduced (lower) symmetry will survive in the dipole–dipole term. At resonance, the intensity of the forbidden reflection is enhanced with increasing temperatures due to the electron–phonon interaction dominant contribution (Kokubun *et al.*, 2001; Kirfel *et al.*, 2002).

In this paper, with the forbidden (002) and weak (222) reflections we measure the phases of structure-factor triplets of three-beam and four-beam diffraction around the Ge *K* edge at various temperatures. The phase shifts at resonance are determined using multiple-beam diffraction techniques.

2. Phase determination of structure-factor triplets

Here we employ the multiple-beam diffraction technique (Hümmer *et al.*, 1990; Chang & Tang, 1988; Lee *et al.*, 2001; Chang, 1998, 2004; Colella & Shen, 2006) to extract the phase information of the involved structure-factor triplets. Multiple-beam diffraction occurs when two or more Bragg reflections are excited at the same time. For an (O, G, L) three-beam diffraction, the crystal is first aligned for a given G reflection as the primary reflection. The crystal is then rotated around the reciprocal-lattice vector $\mathbf{OG}(=\mathbf{g})$ of the G reflection to bring another reciprocal-lattice point, denoted as L, of the secondary reflection onto the surface of the Ewald sphere, thus causing multiple diffraction to take place. This azimuth rotation around **g** is the so-called Renninger scan (Renninger, 1937). Figs. 1(*a*) and 1(*b*) show the diffraction geometries in the real space and reciprocal space, respectively. Point C is the centre of the Ewald sphere. The points O, G and L are the reciprocal-lattice points of the incident, primary and secondary reflections, respectively. $\mathbf{K}_O$, $\mathbf{K}_G$ and $\mathbf{K}_L$ are the wavevectors of the involved diffracted beams inside the crystal. **g** and **l** are the reciprocal-lattice vectors of the G and L reflections. During the azimuthal scan process, there are two positions where the secondary reciprocal-lattice point L could touch the surface of the Ewald sphere, denoted as 'IN' for entering and 'OUT' for leaving the Ewald sphere. One of the diffracted beams in the three-beam case can be treated as a reference for other beams. The interaction among the diffracted beams modifies the intensity of each diffracted beam, including the primary reflection. The intensity variation is closely related to the structure-factor triplet $F_3(=|F_{G-L}||F_{L-O}|/|F_{G-O}|)$ and the triplet phase $\delta_3(=-\delta_{G-O}+\delta_{G-L}+\delta_{L-O})$, where δ_{G-O}, δ_{L-O} and δ_{G-L} are the individual phases of the primary, secondary and coupling reflections, respectively. The triplet phase is independent of the choice of the origin of the unit cell, also called the phase invariant. The modified intensity usually exhibits an asymmetric character, related to the sign of $\cos\delta_3$, on the tails of the multiple-beam diffraction, or *vice versa*. Also the peak intensity depends on

the sign of $\sin\delta_3$. This phase-dependent diffraction profile is well understood according to theoretical consideration based on the dynamical theory. For quantitative phase determination of $\sin\delta_3$ and $\cos\delta_3$, a pair of inversion-symmetry-related (ISR) three-beam diffractions, (O, G, L) and $(O, -G, -L)$, are required (Hümmer *et al.*, 1990; Chang, 1998; Stetsko, Juretschke *et al.*, 2001).

According to the dynamical theory of X-ray diffraction and Born approximation (Chang & Tang, 1988), the relative intensity I'_G can be written as a function of the azimuth angle φ:

$$\begin{aligned} I'_G &= \frac{I_G^{(3)} - I_G^{(2)}}{I_G^{(2)}} \\ &= I_D + I_K \\ &= \frac{ap(2\Delta\varphi\cos\delta_3 - \eta\sin\delta_3)}{(\Delta\varphi)^2 + (\frac{\eta}{2})^2} + \frac{bp^2}{(\Delta\varphi)^2 + (\frac{\eta}{2})^2} \end{aligned} \tag{1}$$

where $p = (|F_{G-L}||F_{L-O}|)/|F_{G-O}|$, the coefficients a and b are proportional constants, and η is the width of the multi-beam diffraction intensity profile. $I_G^{(3)}$ and $I_G^{(2)}$ are the diffraction intensities of the primary reflection G at the three-beam and two-beam positions, respectively. For a pair of ISR three-beam diffractions, (O, G, L) and $(O, -G, -L)$, equation (1) can be rearranged as asymmetrical Lorentzian functions to fit the measured intensity distributions from the two three-beam cases (Stetsko, Lin *et al.*, 2001),

$$L_\pm(\Delta\varphi) = \frac{a_\pm(\Delta\varphi - \Delta\varphi_{0\pm}) - b_\pm}{(\Delta\varphi - \Delta\varphi_{0\pm})^2 + c_\pm^2} \tag{2}$$

where the symbols '+' and '−' represent (O, G, L) and $(O, -G, -L)$ three-beam cases, respectively. Note that to change the diffraction geometry from (O, G, L) to $(O, -G, -L)$, the crystal needs to be turned upside down. $\Delta\varphi_{0\pm}$ are the zero points of the asymmetrical Lorentzian functions. The quantities $a_\pm$ depend on the cosines of the triplet phases $\delta_+ = \delta_{G-L} + \delta_{L-O} - \delta_{G-O}$ and $\delta_- = \delta_{L-G} + \delta_{O-L} - \delta_{O-G}$, respectively, which control the asymmetry of the intensity profile. The quantities $b_\pm$ are related to the sines of $\delta_\pm$ which affect the peak intensities, either peak or dip, of the intensity profiles in the quantitative phase analysis. Usually, $b_\pm < 0$ for an *Umweg*-type and $b_\pm > 0$ for an *Aufhellung*-type multiple diffraction (Chang, 2004). The quantities $c_\pm$ are the widths of the intensity profiles and are larger than zero. The triplet phases can be calculated from the best fit parameters, $a_\pm$, $b_\pm$ and $c_\pm$, according to equations (1)–(2), as

$$\tan\delta_\pm = \frac{b_\pm - b_\mp}{2a_\pm c_\pm}. \tag{3}$$

The quadrants to which the triplet phases $\delta_\pm$ belong are determined by the signs of the numerator and denominator of equation (3). The intensity variations in the azimuthal scans around the diffraction vector of the primary $+G$ and $-G$ in the vicinity of three-beam diffractions are related to the triplet phases $\delta_\pm$. Note that triplet phases $\delta_+ (= \delta_{G-L} + \delta_{L-O} - \delta_{G-O})$ and $\delta_- (= \delta_{L-G} + \delta_{O-L} - \delta_{O-G})$ are the phases of the structure-factor triplets $F_{G-L}F_{L-O}/F_{G-O}$ and $F_{L-G}F_{O-L}/F_{O-G}$, respectively, where δ_H is the phase of the individual H reflection $(H = G, L, G - L)$. The phase sum, called resonance phases (Stetsko, Lin *et al.*, 2001), $\Delta_{G-O} = \delta_{G-O} + \delta_{O-G}$, $\Delta_{L-O} = \delta_{L-O} + \delta_{O-L}$ and $\Delta_{G-L} = \delta_{G-L} + \delta_{L-G}$, are the phases of the structure-factor products $F_{G-O}F_{O-G}$, $F_{L-O}F_{O-L}$ and $F_{G-L}F_{L-G}$, respectively. The triplet resonance phase $\Delta = (\delta_+ + \delta_-)/2 \equiv (-\Delta_{G-O} + \Delta_{L-O} + \Delta_{G-L})/2$ is an average of the sum of the triplet phases involved. Far from the absorption edge, the two ISR three-beam diffractions (O, G, L) and $(O, -G, -L)$ give zero values for Δ_{G-O}, Δ_{L-O}, Δ_{G-L} and the triplet resonance phase Δ due to negligibly small anomalous dispersion corrections. At the absorption edge, Friedel's law is invalid and the asymmetric behaviours in intensity profiles become pronounced; the same is true for the peak intensities. All of the resonance phases have significant contributions to the anomalous behaviour of X-ray multi-beam diffraction.

For a four-beam diffraction, the phases of the dominant structure-factor triplets can be determined as in three-beam cases, provided that the primary reflection involves a 2 or 2_1 rotational symmetry (Hümmer *et al.*, 1990; Chang & Tang, 1988; Chang, 1998, 2004).

3. Experiment

The experiments were carried out at the Taiwan beamline BL12B2 at SPring-8, Japan. The germanium crystals were commercial products in the form of wafers with two-sided polished surfaces and the orientation of the large surface was chosen to be a [001]- and [111]-cut plane to execute multiple-beam X-ray diffraction experiments. The incident photon energy was tuned around the germanium absorption K edge (= 11103 eV) by a Si(111) double-crystal monochromator (DCM). Upstream of the DCM, a mirror coated with Rh was used to suppress mostly high-order signals of the required photon flux entering the Si(111) DCM. Downstream of the DCM, the horizontal and vertical of the incident beam were focused by a toroidal mirror. The beam size was then set by slits with 0.2 × 0.2 (H × V) mm at the sample position. The incident photon energy was calibrated by a germanium absorption spectrum with an energy interval of 0.25 eV. Before collecting experimental data, we needed to ensure there was no contamination of the incident signals with high-order harmonics. We rocked the second crystal of the DCM Si(111) and monitored the Gaussian profile of the incident beam from an ion chamber (I0), and temporarily moved the motor to the peak position of the measured profile. In order to avoid the high-order harmonic signals being absorbed by an attenuator, we then measured the forbidden reflection at the resonant energy without the attenuator, and obtained the full signals including the high-order harmonics. All of them were exhibited on the screen of an oscilloscope. Choosing a suitable operating voltage range for the scintillation counter, correct signals for the measured intensity were picked up. Then the line profile of the Si(111) DCM was detuned to about 80% of

its maximum intensity. The detuned direction of the second crystal of the DCM was away from the angular peak position of the half-wavelength.

4. (002) and (222) reflections at room temperature

The Ge crystal was mounted on a cryostat, which was placed at the centre of a four-circle diffractometer. The mirror symmetries appearing in multiple-beam diffraction patterns were determined by performing a Renninger scan, the φ scan, around the reciprocal-lattice vector [002], where the position coincided with the plane of incidence, usually defined as $\varphi = 0^\circ$. For convenience, we assigned $\varphi = 0^\circ$ at the resonant two-beam diffraction peak position. The integrated intensity of the forbidden reflection (002) was measured at energies across the Ge absorption K edge (= 11103 eV), shown in Fig. 2(a). After the peak position ($E \sim E_K$) the integrated intensity of the (002) reflection gradually decreased when the incident photon energy was away from the resonant conditions. As a result, the (002) reflection displayed the pure resonance character. The (222) reflection was also space-group forbidden. However, due to aspherical electron-density distribution (Roberto *et al.*, 1974), the so-called covalent bond (Phillips, 1968), nonzero diffraction intensity was observed. The interatomic electrons are the source of scattering for the (222) reflection. The integrated intensity of the (222) reflection, Fig. 2(b), can still be detected under the non-resonant conditions due to aspherical electron density and atomic thermal motion. The spectral distribution of the (222) reflection shows a dip near the resonant energy because of the rapidly increased linear absorption coefficient and weak intensity contributions near the absorption edge. This is in agreement with the results reported in the literature (Mukhamedzhanov *et al.*, 2007) where the dipole–quadrupole and thermally induced contributions are important.

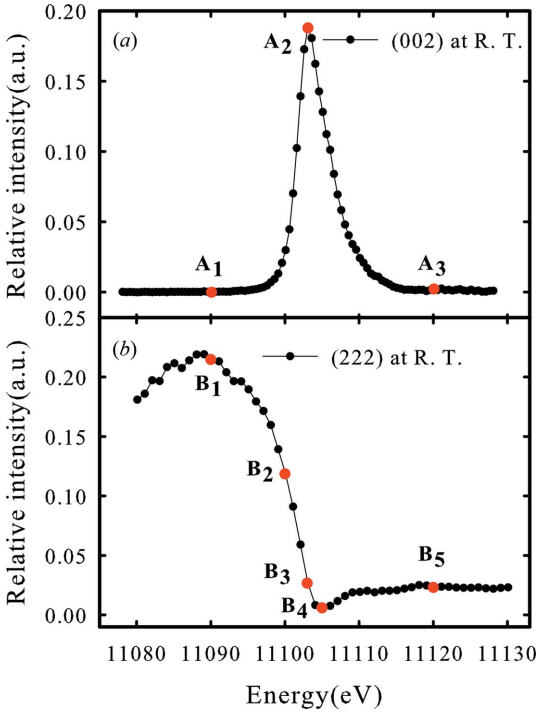

Figure 2
(a) The energy dependence of the (002) reflection intensity measured at room temperature. The solid red circles labelled with A_1, A_2 and A_3 represent the photon energies 11090, 11103 and 11120 eV, respectively. (b) The energy dependence of the (222) reflection intensity at room temperature. The symbols B_1, B_2, B_3, B_4, B_5 indicate 11090, 11102, 11103, 11105 and 11120 eV, respectively.

5. Three-beam and four-beam diffraction at room temperature

Figs. 3(a)–3(c) show the intensity profiles of Ge (002) at the four-beam diffraction positions near the germanium absorption K edge at room temperature for the two ISR cases, '+' (000)(002)(375)(37$\bar{3}$) and '−' (000)(00$\bar{2}$)($\bar{3}\bar{7}\bar{5}$)($\bar{3}\bar{7}$3), where (000) is the incident reflection, (002) and (00$\bar{2}$) are, respectively, the ISR primary reflections. The intensity profiles were obtained at the energies marked by the solid red circles with symbols A_1, A_2, A_3 as shown in Fig. 2(a). Referring to Fig. 3(a) for 11090 eV, the intensity of the left tail of the '+' four-beam diffraction (see the solid circle curve) is higher than that of the right tail. This intensity asymmetry indicates that $\cos\delta_+ < 0$. The same is true for the tails for the '−' four-beam case (see the open-circle curve); hence $\cos\delta_- < 0$. Also the peak intensity of the '+' four-beam case is higher than that of the '−' case. This implies that $\sin\delta_+ < 0$ and $\sin\delta_- > 0$. The quantitative phase analysis leads to $\delta_+ = -99.1^\circ$, $\delta_- = 99.7^\circ$ and triplet resonance phase $\Delta = (\delta_+ + \delta_-)/2 = 0.3^\circ$. At the Ge K edge, 11103 eV, the tail asymmetries of both '+' and '−' cases

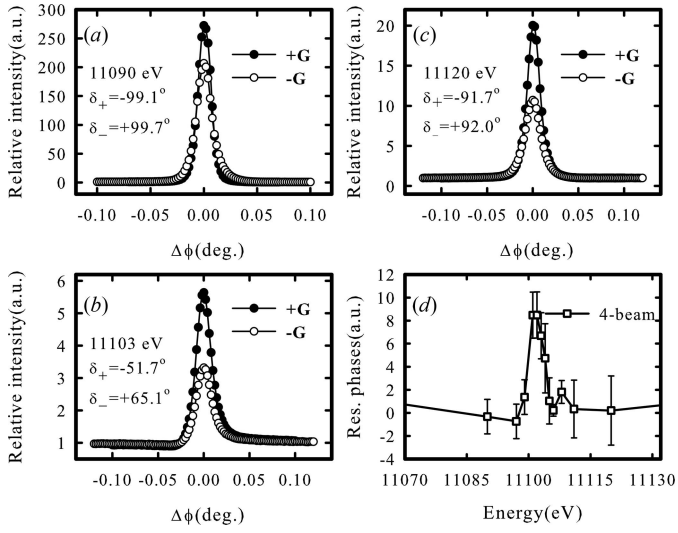

Figure 3
The (002) intensity profiles of ISR four-beam diffractions, (000)(002)(375)(37$\bar{3}$) ('+' case) and (000)(00$\bar{2}$)($\bar{3}\bar{7}\bar{5}$)($\bar{3}\bar{7}$3) ('−' case) at room temperature near the Ge K edge. Profiles (a)–(c) were obtained at the energies indicated in Fig. 2(a) by solid red circles. Intensities were normalized by the average of the intensity background from the right- and left-hand of the four-beam intensity profiles. Solid circles for '+' case; open circles for '−' case. (d) The spectral distribution of the resonance triplet phases of the four-beam cases is displayed with open black squares.

are reversed, *i.e.* the left tail is lower than the right tail (Fig. 3*b*), namely, $\cos\delta_+ > 0$ and $\cos\delta_- > 0$. Also the peak intensity of the '+' case is higher than that of the '−' case, indicating that $\sin\delta_+ < 0$ and $\sin\delta_- > 0$. This gives $\delta_+ = -51.7^\circ$, $\delta_- = 65.1^\circ$ and triplet resonance phase $\Delta = 6.7^\circ$. In other words, the overall asymmetry of the intensity profiles observed for the two ISR cases is reversed when the energy crosses the Ge *K* edge. In addition, the fitting parameters, $a_\pm$ in equation (2), have negative values at non-resonance energies but change their signs at resonance. When the photon energy is above E = 11111 eV, the asymmetry profiles of the four-beam diffraction are recovered, similar to the initial profiles at E = 11090 eV (Fig. 3*a*). Fig. 3(*c*) shows the same intensity asymmetry at 11120 eV. As shown in Fig. 3(*d*), the resonance triplet phase of the four-beam case at room temperature is about 8.3° for 11102 eV (not shown here) due to electronic transitions and decreases to zero when the incident photon energy is far from the Ge *K* edge.

Figs. 4(*a*)–4(*e*) display the room-temperature intensity profiles of the (222) at three-beam diffraction near the Ge absorption *K* edge for the two ISR cases, '+' (000)(222)($\bar{5}3\bar{3}$) and '−' (000)($\bar{2}\bar{2}\bar{2}$)(5$\bar{3}$3). The energies in Figs. 4(*a*)–4(*e*) are marked as solid red circles with symbols B_1, B_2, B_3, B_4, B_5 in Fig. 2(*b*). As shown in Fig. 4(*a*) for 11090 eV and Fig. 4(*b*) for 11102 eV, the tail intensity asymmetries are such that the left tails are lower than the right tails, indicating that $\cos\delta_+ > 0$ and $\cos\delta_- > 0$. However, the asymmetry of Fig. 4(*b*) is more pronounced than that of Fig. 4(*a*). Also the peak intensities of both figures give $\sin\delta_+ > 0$ and $\sin\delta_- < 0$. The determined phases are $\delta_+ = 79.3^\circ$, $\delta_- = -73.9^\circ$ and triplet resonance phase $\Delta = 2.7^\circ$ for 11090 eV and $\delta_+ = 8.3^\circ$, $\delta_- = -6.7^\circ$ and triplet resonance phase $\Delta = 0.8^\circ$ for 11102 eV. As can be seen, the triplet phases of the latter (Fig. 4*b*) are close to 0°, giving typical sharp asymmetric profiles. When the photon energy crosses the Ge *K* edge, the tail asymmetry of Fig. 4(*c*) for 11103 eV is reversed compared to Fig. 4(*b*). Also the triplet phases are changed from 0° to nearly 180°. The resonance triplet phase is changed slightly from $\Delta = 0.8^\circ$ to $\Delta = -1.9^\circ$. Moreover, the fitting parameters, $a_\pm$, change thier signs from positive at non-resonance to negative at resonance. When the energy reaches E = 11105 eV, the asymmetry of the intensity profiles returns to the initial situations prior to the resonance (Figs. 4*a*, 4*e*). The resonance triplet phase of the three-beam case at room temperature is about −19.5° for 11105 eV and returns to close to 0° afterward, as shown in Fig. 4(*f*).

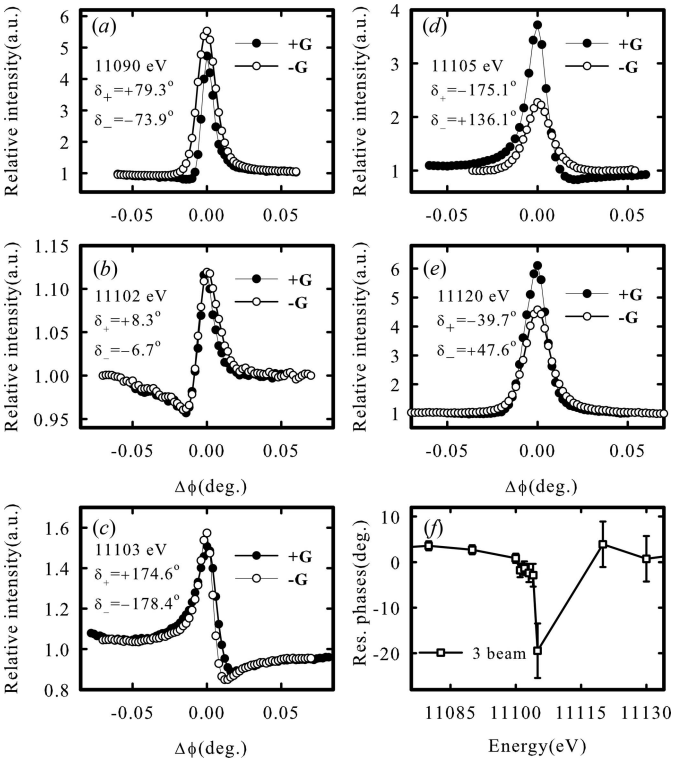

Figure 4
The (222) intensity profiles of ISR four-beam diffractions, (000)(222)($\bar{5}3\bar{3}$) ('+' case) and (000)($\bar{2}\bar{2}\bar{2}$)(5$\bar{3}$3) ('−' case) at room temperature near the Ge *K* edge. Profiles (*a*)–(*e*) were obtained at the energies indicated in Fig. 2(*b*) by solid red circles. Intensities were normalized by the two-beam intensity which was obtained from the intensity average of the right- and left-hand of the three-beam intensity profiles. Solid circles: '+' case; open circles: '−' case. (*f*) The spectral distribution of the resonance triplet phases of the three-beam case.

6. (002) and (222) reflections at low temperatures

The intensities of the (002) and (222) reflections at E = 11103 eV were measured when the crystal was cooled from T = 300 K to T = 20 K. As shown in Fig. 5, the (002) reflection intensity at resonance has nonzero intensity due to temperature-dependent thermally induced contributions. The latter give rise to structure-factor anisotropy. Atomic thermal motions in Ge cause the electron density of the resonant atom to couple strongly with neighbouring atoms and enhance the Bragg reflection. The intensity of the (002) reflection at E = 11053 eV becomes detectable at the low temperature T = 20 K due mainly to Debye–Waller factor contributions. However, the curve of open circles in Fig. 5 showing that the intensity at 20 K is higher than that at higher temperatures is probably due partly to the long-range tails of multi-beam diffraction contributing to the relatively weak (002) intensities. On the

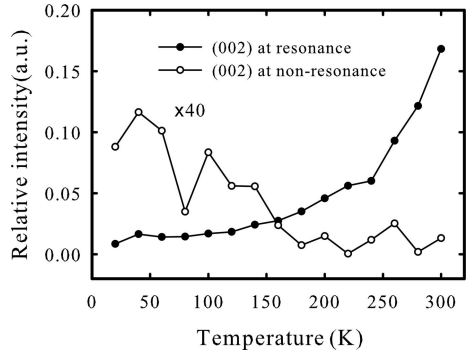

Figure 5
The temperature dependence of the (002) reflection intensity at the resonance energy 11103 eV (solid circles) and non-resonance energy 11053 eV (open circles, the intensity scale was multiplied 40 times).

other hand, the curve with solid curves shows the thermally induced contribution, *i.e.*, the stronger the intensity the higher the temperature. The thermally induced contribution in the forbidden reflection (002) is dominant.

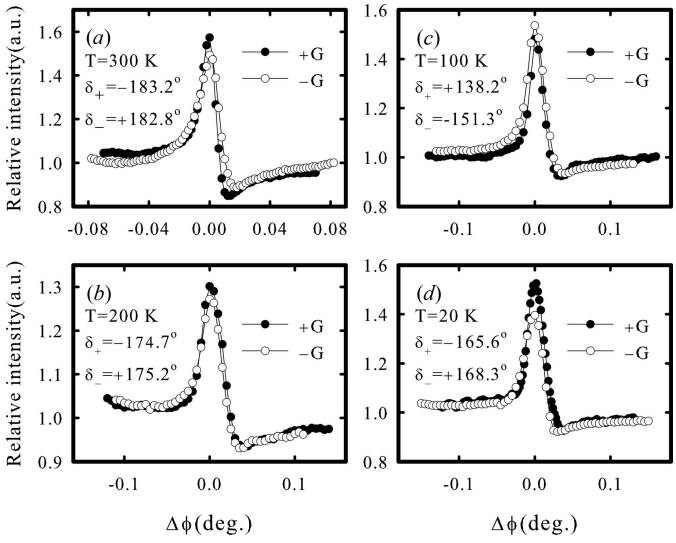

Figure 6
The (222) intensity profiles of ISR four-beam diffractions, (000)(222)($\bar{5}\bar{3}\bar{3}$) ('+' case) and (000)($\bar{2}\bar{2}\bar{2}$)($\bar{5}\bar{3}\bar{3}$) ('−' case), were measured at resonance at low temperatures: (*a*) T = 300 K, (*b*) T = 200 K, (*c*) T = 100 K and (*d*) T = 20 K (solid circles: '+' case; open circles: '−' case).

7. Resonance triplet phases of mutiple-beam diffraction at low temperatures

The (222) intensity profiles of the ISR three-beam diffractions, '+' (000)(222)($\bar{5}\bar{3}\bar{3}$) and '−' (000)($\bar{2}\bar{2}\bar{2}$)($5\bar{3}\bar{3}$), were measured at resonance, *i.e.* E = 11103 eV at T = 20, 100, 200 and 300 K, as shown in Fig. 6. The tail asymmetries of Figs. 6(*a*)–6(*d*) are almost the same, namely the left tails are higher than the right ones, indicating that $\cos\delta_+ < 0$ and $\cos\delta_- < 0$. However, the peak intensities show that the intensity of the '+' case is nearly equal to that of the '−' case for T = 300 K (Fig. 6*a*). This leads to $\delta_+ \sim \delta_- = 180°$ and the resonant phase shift nearly equals zero, *i.e.* $\Delta = -0.2°$. When the temperature reaches 200 K, the peak intensity of the '−' case decreases slightly compared to that of the '+' case (Fig. 6*b*), which gives $\delta_+ = -174.7°$ and $\delta_- = 175.2°$ and the resonant phase shift $\Delta = 0.25°$. At T = 100 K (Fig. 6*c*), the peak intensity of the '−' case becomes higher than that of the '+' case, meaning that $\delta_+ = 138.2°$ and $\delta_- = -151.3°$ and $\Delta = -6.6°$. When the temperature is 20 K, the peak intensity of the '−' case becomes much lower than that of the '+' case (Fig. 6*d*), which gives $\delta_+ = -165.6°$ and $\delta_- = 168.3°$ and $\Delta = 1.4°$. Considering the overall experimental and calculation errors in phase determination, the effects of temperature dependence of triplet phases and resonance phases are relatively small. The error in the experimentally determined phase is estimated to be about $\pm$ 5°.

The (002) intensity profiles of the two ISR four-beam diffractions, '+' (000)(002)(375)(37$\bar{3}$) and '−' (000)(00$\bar{2}$)($\bar{3}\bar{7}\bar{5}$)-

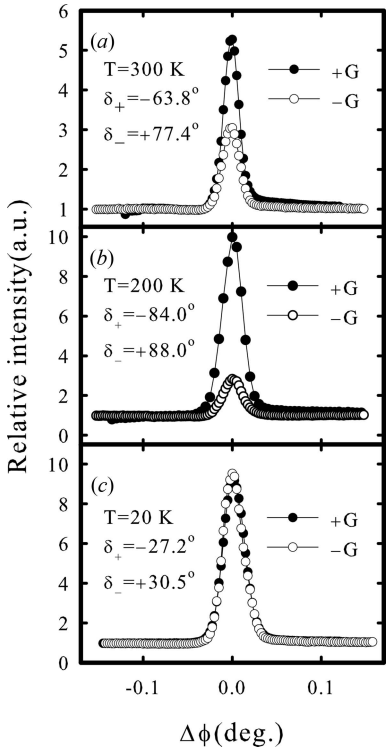

Figure 7
The (002) intensity profiles of ISR four-beam diffractions, (000)(002)(375)(37$\bar{3}$) ('+' case) and (000)(00$\bar{2}$)($\bar{3}\bar{7}\bar{5}$)($\bar{3}\bar{7}\bar{3}$) ('−' case), were measured at resonance at low temperatures: (*a*) T = 300 K, (*b*) T = 200 K, (*c*) T = 20 K (solid circles: '+' case; open circles: '−' case).

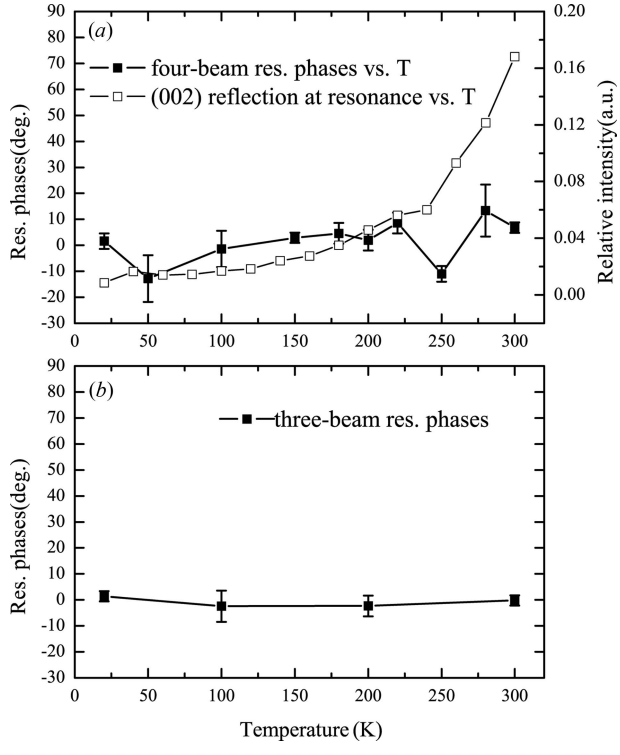

Figure 8
The resonance triplet phases of (*a*) the four-beam case (000)(002)(375)(37$\bar{3}$) [the intensity of the (002) reflection at resonance *versus* temperature serves as a reference] and of (*b*) the three-beam case (000)(222)($\bar{5}\bar{3}\bar{3}$) *versus* temperature.

($\overline{3}73$), were measured at resonance (11103 eV) for $T = 20$, 200 and 300 K, as shown in Fig. 7. The intensity profiles in Figs. 7(*a*)–7(*c*) all show slightly lower intensity of the left tail than that of the right one, indicating that $\cos\delta_+ > 0$ and $\cos\delta_- > 0$. However, the peak intensities of the '−' case at 200 K and 300 K are nearly the same and increased to more than double at 20 K. This is because, according to equation (1), the intensity variation is related to the structure-factor triplets *p*. The stronger the intensity variation, the weaker the (002) two-beam intensity. That is, when the temperature is lowered to 20 K, the (002) intensity is very weak (see the resonant curve in Fig. 5). This leads to $\delta_+ = -27.2°$ and $\delta_- = 30.5°$ and $\Delta = 1.7°$ for the low temperature (20 K), compared to $\delta_+ = -84°$ and $\delta_- = 88°$ and $\Delta = 2°$ for 200 K and $\delta_+ = -63.8°$ and $\delta_- = 77.4°$ and $\Delta = 6.8°$ for room temperature (300 K).

The resonance triplet phases measured from the three-beam and four-beam diffraction are plotted against temperature from 20 K to 300 K in Fig. 8. The two-beam intensities of (002) at resonance are also displayed as a reference for the four-beam measurements in Figs. 8(*a*) and 8(*b*). Although the two-beam intensities of (002) show an increasing trend as temperature increases, the resonance triplet phases of the three-beam and four-beam diffraction seem to change very little. The variation of resonance phases is within about 0–7°.

8. Conclusion

We have shown that use of the forbidden/weak reflection as the primary reflection is sensitive enough to provide phase information from multiple-beam diffraction measurements on Ge when the incident photon energy crosses the Ge absorption *K* edge. With the Renninger scan both the three- and four-beam cases have clearly shown a change in intensities due to triplet phases as a function of photon energy. Although the two-beam (002) reflection intensity shows strong effects due to thermally induced anisotropy, the measured resonance triplet phases of both (002)-based four-beam cases and (222)-based three-beam cases seem to show less effects with thermal motion. One of the reasons is probably that in the diffraction processes only (002) is an ATS reflection and the rest of the secondary and coupling reflections are not. Nevertheless, the Renninger scan is still very useful for providing information about triplet phases, in addition to diffracted intensities. It should also be noted that the atomic scattering factors of an ATS reflection are of tensor form (Dmitrienko, 1983). The amplitude and phase could be measured with respect to appropriate polarizations. However, because of the fact that in a multiple-beam diffraction the relations between the polarized wave amplitudes of involved reflections are rather complicated, the measured intensities and phases, including the resonance triplet phases of the current experiments, could be considered as averaged quantities over polarization. Ideally, the use of analysers for the diffracted beams for each polarization would serve this purpose. Moreover, to study highly correlated systems, involving charge and orbital ordering, multiple-beam diffraction at resonance or MDAFS (multi-beam diffraction anomalous fine structure; Lee *et al.*, 2006), together with appropriate calculation schemes for tensorial atomic scattering factors, like FDMNES (finite difference method near-edge structure; Joly, 2001), could be very useful in delineating the atomic, electronic and magnetic properties of a material.

Acknowledgements

We are grateful to the Ministry of Science and Technology and the Ministry of Education for financial support. Technical support from the Synchrotron Radiation Research Center and Spring-8 is also acknowledged.

References

Chang, S.-L. (1998). *Acta Cryst.* A**54**, 886–894.
Chang, S.-L. (2004). *X-ray Multiple-wave Diffraction: Theory and Application*, ch. 7. Berlin: Springer-Verlag.
Chang, S.-L. & Tang, M.-T. (1988). *Acta Cryst.* A**44**, 1065–1072.
Colella, R. & Shen, Q. (2006). *Acta Cryst.* A**62**, 459–462.
Dmitrienko, V. E. (1983). *Acta Cryst.* A**39**, 29–35.
Dmitrienko, V. E. (1984). *Acta Cryst.* A**40**, 89–95.
Dmitrienko, V. E. & Ovchinnikova, E. N. (2000). *Acta Cryst.* A**56**, 340–347.
Dmitrienko, V. E., Ovchinnikova, E. N. & Ishida, K. (1999). *JETP Lett.* **69**, 938–942.
Hümmer, K., Weckert, E. & Bondza, H. (1990). *Acta Cryst.* A**46**, 393–402.
Joly, Y. (2001). *Phys. Rev. B*, **63**, 125120.
Kirfel, A., Grybos, J. & Dmitrienko, V. E. (2002). *Phys. Rev. B*, **66**, 165202.
Kokubun, J., Ishida, K., Cabaret, D., Mauri, F., Vedrinskii, R. V., Kraizman, V. L., Novakovich, A. A., Krivitskii, E. V. & Dmitrienko, V. E. (2004). *Phys. Rev. B*, **69**, 245103.
Kokubun, J., Kanazawa, M., Ishida, K. & Dmitrienko, V. E. (2001). *Phys. Rev. B*, **64**, 073203.
Lee, T. L., Felici, R., Hirano, K., Cowie, B., Zegenhagen, J. & Colella, R. (2001). *Phys. Rev. B*, **64**, 201316.
Lee, Y.-R., Stetsko, Y. P., Sun, W.-H., Weng, S.-C., Cheng, S.-Y., Lin, G.-G., Soo, Y.-L. & Chang, S.-L. (2006). *Phys. Rev. Lett.* **97**, 185502.
Mukhamedzhanov, E. K., Borisov, M. M., Morkovin, A. N., Antonenko, A. A., Oreshko, A. P., Ovchinnikova, E. N. & Dmitrienko, V. E. (2007). *JETP Lett.* **86**, 783–787.
Phillips, J. C. (1968). *Phys. Rev.* **166**, 832–838.
Renninger, M. (1937). *Z. Kristallogr.* **106**, 141–176.
Roberto, J. B., Batterman, B. W. & Keating, D. T. (1974). *Phys. Rev. B*, **9**, 2590–2599.
Stetsko, Yu. P., Juretschke, H. J., Huang, Y.-S., Lee, Y.-R., Lin, T.-C. & Chang, S.-L. (2001). *Acta Cryst.* A**57**, 359–367.
Stetsko, Y. P., Lin, G.-Y., Huang, Y.-S., Chao, C.-H. & Chang, S.-L. (2001). *Phys. Rev. Lett.* **86**, 2026–2029.
Templeton, D. H. & Templeton, L. K. (1980). *Acta Cryst.* A**36**, 237–241.
Templeton, D. H. & Templeton, L. K. (1994). *Phys. Rev. B*, **49**, 14850–14853.